NASA Technical Memorandum 100779

Numerical Modeling of Multidimensional Flow in Seals and Bearings Used in Rotating Machinery

R.C. Hendricks
Lewis Research Center
Cleveland, Ohio

L.T. Tam and A. Przekwas
CHAM
Huntsville, Alabama

A. Muszynska
Bently Rotordynamics Research Corporation
Minden, Nevada

M.J. Braun
University of Akron
Akron, Ohio

R.L. Mullen
Case Western Reserve University
Cleveland, Ohio

Prepared for the
2nd International Symposium on Transport Phenomena, Dynamics, and Design of Rotating Machinery
cosponsored by the ASME and JSME
Honolulu, Hawaii, April 4-6, 1988

NASA

NUMERICAL MODELING OF MULTIDIMENSIONAL FLOW IN SEALS AND BEARINGS USED IN ROTATING MACHINERY

R.C. Hendricks
National Aeronautics and Space Administration
Lewis Research Center
Cleveland, Ohio 44135

L.T. Tam and A. Przekwas
CHAM
Huntsville, Alabama 35816

A. Muszynska
Bently Rotordynamics Research Corporation
Minden, Nevada 89423

M.J. Braun
University of Akron
Akron, Ohio 44325

R.L. Mullen
Case Western Reserve University
Cleveland, Ohio 44106

E-3909

SUMMARY

The rotordynamic behavior of turbomachinery is critically dependent on fluid dynamic rotor forces developed by various types of seals and bearings. The occurrence of self-excited vibrations often depends on the rotor speed and load. Misalignment and rotor wobbling motion associated with differential clearance have often been attributed to stability problems. In general, the rotative character of the flowfield is a complex three-dimensional system with secondary flow patterns that significantly alter the average fluid circumferential velocity. A multidimensional, nonorthogonal, body-fitted-grid fluid flow model is presented that describes the fluid dynamic forces and the secondary flow pattern development in seals and bearings. Several numerical experiments were carried out to demonstrate the characteristics of this complex flowfield. Analyses were performed by solving a conservation form of the three-dimensional Navier-Stokes equations transformed to those for a rotating observer and using the general-purpose computer code PHOENICS with the assumptions that the rotor orbit is circular (nonzero dynamic eccentricity) and that static eccentricity is zero. These assumptions have enabled a precise steady-state analysis to be used.

Fluid injection from ports near the seal or bearing center increased fluid-film direct dynamic stiffness ($K_D = K - M\omega^2(1 - \lambda \pm \lambda_e)$) and, in some cases, significantly increased quadrature dynamic stiffness ($K_Q = D\omega(1 - \lambda \pm \lambda_e) - K_{XY}$). Under certain conditions K_Q was less than zero, implying instability (necessary but not sufficient condition) and geometric configuration dependency (refs. 1 and 2). Injection angle and velocity could be used for active rotordynamic control; for example, injection, when compared with no injection, increased direct dynamic stiffness, which is an important factor for hydrostatic bearings.

Three turbulence models were tested: Prandtl mixing, standard k-ε, and modified k-ε. The Prandtl model underpredicted and the standard k-ε model overpredicted secondary flow zone. The modified k-ε model was postulated to provide better predictions of secondary flow zones and dynamic stiffness (direct and quadrature).

The Richardson parameter related turbulence production and dissipation within the passage; positive Richardson numbers were associated with zones of secondary flow and represented regions where turbulence dissipation exceeded production, an important observation for stable seal and bearing designs. Designs should provide low production near the stator.

INTRODUCTION

The characterization of turbulence in high shear flows is at best difficult, perhaps impossible. Such flows can and do occur within the passages of rotating cylindrical configurations with or without axial pressure drop. For industrial applications these passages represent seals and bearings, respectively, but could equally well represent high-speed propulsion systems or ballistic projectiles. A major difference between characterizing high-shear flows in rotating systems and those of an airframe, for example, is the development of centrifugal and Coriolis forces and the coupling between an unsteady energy source and the working fluid.

In turbulence modeling of high-shear flows (seals or bearings) researchers assume the validity of the universal friction laws, which are based on low-shear-flow data. Such modeling ranges from indirect inference of irreversible momentum loss to production and dissipation mechanisms. For example, Bentley et al. (ref. 3) use a rotordynamic model with a bulk flow parameter to characterize circumferential velocity (indirectly related to wall or fluid shear); Nelson and Nguyen (ref. 4) use gas dynamics equations with Hirs' bulk model for friction; Tam et al. (ref. 5) use Prandtl's model; Nordman et al. (ref. 6) use the standard k-ε model. Each researcher obtained good agreement with the experimental data of Childs (ref. 7). Such agreement is necessary but not sufficient to justify a model or to characterize the turbulence of high shear flows.

This paper compares three models, Prandtl, standard k-ε, and modified k-ε, and relates the results, along with fluid injection, to seal and bearing dynamics. The characterization of turbulence is not established as the Navier-Stokes solver uses wall functions, derived from the universal law, and coarse grid in the near-wall region (NX x NY x NZ = 12 x 6 x 16).

SYMBOLS

C_d	empirical constant
D	damping coefficient, N s/m
E	constant (integrated function of surface roughness)
K_D	fluid-film direct dynamic stiffness, $K - M\omega^2(1 - \lambda \pm \lambda_e)$, N/m

K_Q	fluid-film quadrature dynamic stiffness, $D\omega(1 - \lambda \pm \lambda_e) - K_{xy}$, N/m
K_{xy}	cross-coupled stiffness, N/m
k	turbulence production parameter, $(m/s)^2$
M	mass, kg
NX,NY,NZ	node spacing
P_k	production of turbulence kinetic energy, eq. (4), kg/m s^3
Ri	Richardson parameter
S_ε	turbulence dissipation source term, kg/m s^4
S_{kP}; S_{kI}	production source terms in two-equation model, kg/m s^3
$S_{\varepsilon P}$; $S_{\varepsilon I}$	dissipation source terms in two-equation model, kg/m s^4
t	time, s
u	velocity, m/s
u_θ	circumferential velocity, m/s
$\langle u \rangle$	average velocity, m/s
x, y, r	coordinates, m
ε	turbulence dissipation parameter, m^2/s^3
κ	von Karman constant
λ	average velocity parameter
λ_e	injection or preswirl average velocity parameter
μ	viscosity, kg/m s or Pa s
ρ	density, kg/m^3
σ_k	production Prandtl number
σ_ε	dissipation Prandtl number
τ	wall shear stress, Pa
ω_p	perturbation angular speed, rad/s
ω_R	rotational angular speed, rad/s

TURBULENCE MODELS USED IN SIMPLE TURBULENT FLOWS

Turbulent flows are generally modeled by using a two-equation k-ε turbulence model (refs. 8 and 9). In the k-ε model the local state of turbulence is characterized by two scalar quantities, viz, turbulence kinetic energy k and its dissipation rate ε. The local turbulent eddy viscosity μ_t is computed from k and ε as follows:

$$\mu_t = \rho C_d \frac{k^2}{\varepsilon} \tag{1}$$

where ρ is the fluid density and C_d an empirical constant (ref. 8), all derived from flat-plate data assumed to be in local equilibrium. Both k and ε are here supposed, as in the original publications (refs. 8 and 9), to be governed by conventional "transport" equations:

$$\rho \frac{Dk}{Dt} = \frac{\partial}{\partial x_i}\left(\frac{\mu_t}{\sigma_k}\frac{\partial k}{\partial x_i}\right) + P_k - \rho\varepsilon \tag{2}$$

$$\rho \frac{D\varepsilon}{Dt} = \frac{\partial}{\partial x_i}\left(\frac{\mu_t}{\sigma_\varepsilon}\frac{\partial \varepsilon}{\partial x_i}\right) + \frac{\varepsilon}{k}(C_1 P_k - C_2 \rho\varepsilon) \tag{3}$$

$$P_k = \mu_t \left(\frac{\partial u_i}{\partial x_j} + \frac{\partial u_j}{\partial x_i}\right)\frac{\partial u_j}{\partial x_i} \tag{4}$$

The empirical constants used in the calculations are those recommended in the original references (refs. 8 and 9), $C_1 = 1.44$, $C_2 = 1.92$, $C_d = 0.09$, $\sigma_k = 1.0$, and $\sigma_\varepsilon = 1.3$. This model has been applied to seals with good results (ref. 4).

Boundary Conditions at Wall

For flows near walls it can be presumed (1) that the velocity profile obeys the universal logarithmic law for smooth walls and includes a rough-to-smooth correlation adjustment for wall roughness, (2) that the turbulence energy is proportional to the wall shear stress, and (3) that the length scale is proportional to the distance from the wall.

$$\frac{u}{\sqrt{\tau/\rho}} = \frac{1}{\kappa} \ln\left[E \frac{\rho y \sqrt{\tau/\rho}}{\mu}\right] \tag{5}$$

$$k = \frac{\tau/\rho}{\sqrt{C_d}} \tag{6}$$

$$\varepsilon = \frac{C_d k^2}{(\kappa y \sqrt{\tau/\rho})} \tag{7}$$

where the wall shear stress τ is determined from the velocity u in the near-wall region and $\kappa = 0.435$.

Influence of Curvatures and Swirls on Turbulent Flows

Experimental investigations of flows with significant streamline curvatures, swirling flows in particular, reveal that the extra centrifugal and Coriolis forces can have a surprising effect on turbulence structure and mean flow patterns (ref. 10). It has been observed that turbulence is generally augmented near the concave and reduced near the convex surface of curved channels. Figure 1(a) illustrates the typical swirling velocity profile in a curved channel and indicates the relation between the gradient du/dr of the swirl velocity and the turbulence intensity (i.e., $du/dr < 0$ and $du/dr > 0$). Reduced outward diffusion of turbulence kinetic energy from the convex inner wall, as well as the net force of both the radial pressure gradient and the centrifugal force, prevent the formation of large-scale turbulence. The effect of the concave wall is just the opposite.

In forced swirl, such as that formed by a rotating shaft (fig. 1(b)), the centrifugal forces near the inner wall support the growth of vortical structures even more than in curved-channel flow. The angular velocity gradients are generally negative all across the flowpath, with the largest absolute values near the stator. It is in that region where the largest turbulence will be generated, the "separated" region (fig. 1(b)). This situation is inherently unstable since high turbulence levels weaken the secondary flow patterns. However, introducing preswirl or multiinjection in the seal or bearing configuration can often cause a counterswirling vortex to form near the housing wall. This has been known in practice to have a stabilizing effect on seal, bearing, and rotor dynamics (ref. 5). In this case the largest angular velocity gradient is shifted inward toward the shaft. Within the countervortex zone the Richardson parameter and the gradient of angular velocity change sign, reducing the turbulence levels in that region and enhancing the system stability.

The Modified k-ε Turbulence Model

Existing turbulence models (refs. 8 and 11) can successfully predict only simple boundary layer or mildly recirculating flows. For coupled swirling flows they fail to capture the essential physics of usually anisotropic, nonhomogeneous, and three-dimensional turbulence structures. Reported attempts at predicting rotating turbulent flows indicate that complex, full Reynolds stress equations provide no better predictions than those obtained with simple corrections to the k-ε model (ref. 11). The general consensus is that the empirical constants in semiempirical models (such as standard k-ε) are invalid for complex flows.

For this reason the authors' previous publication (ref. 5), where a simple Prandtl mixing-length model was used to represent the turbulence in seal and bearing flow passages, may not be correct. Herein an attempt was made to evaluate a modified k-ε model and compare its results with those of Prandtl mixing-length and standard k-ε models.

Several investigators have attempted to extend both algebraic Reynolds stress (ARS) and k-ε models to turbulent rotating flows. For a comprehensive review consult the work of Lakshminarayana (ref. 11).

Most of the relevant approaches are based on Bradshaw's suggestion (ref. 10) that the streamline curvature effects can be modeled by modifying the turbulence length scale. Two most relevant approaches are those of Rodi (ref. 9) and Launder et al. (ref. 12). Both incorporate the "rotating" correction into constants of the turbulence dissipation rate source term, viz,

$$S_\varepsilon = \frac{\varepsilon}{k}\left(C_1 P_k - C_2 \rho \varepsilon\right) \tag{8}$$

where P_k is the generation of turbulence kinetic energy k and $C_1 = 1.44$ and $C_2 = 1.92$ are the "universal" constants. Rodi's extension introduces a correction to the model constant C_1 in the generation part of the ε-equation source term:

$$C_1^* = C_1(1 + C_1' Ri) \tag{9}$$

Launder's extension modifies the destruction part of the ε-equation source term in a similar manner by modifying the C_2 constant as

$$C_2^* = C_2(1 + C_2' Ri) \tag{10}$$

where $C_1' = 0.9$ and $C_2' = 0.2$, respectively, and Ri is the Richardson parameter. The models differ in their specifications of the Richardson parameter, which they define as

$$Ri = 2u_\theta \frac{d\left(\frac{u_\theta}{r}\right)}{dr} \frac{\mu_t}{P_k} \qquad \text{Rodi (modifies } C_1\text{)} \tag{11}$$

$$Ri = \left(\frac{k}{\varepsilon}\right)^2 \left(\frac{u_\theta}{r^2}\right) \frac{d(ru_\theta)}{dr} \qquad \text{Launder (modifies } C_2\text{)} \tag{12}$$

Both respond to the angular speed u_θ/r^2, the swirl velocity gradient, and the turbulence time scale, which differs in preceding definitions.

Both approaches were also recently compared by Chen (ref. 13) for confined swirl jet flow, with the conclusion that Launder's correlation gives the best prediction in the recirculating zone. This approach was also used in the present analysis.

Present Analysis

Analysis of the correcting factor indicates that in the regions of negative velocity gradients, Ri is also negative and smaller ε decay intensifies the turbulence level. The negative Richardson parameter starts increasing from the shaft surface, and its magnitude becomes maximum in the separation region. Then the gradient of the Richardson parameter drops sharply and changes to the positive Ri parameter, where the turbulence level is damped and a secondary recirculating zone appears.

Current Development of Turbulence Models

The comparative verification studies of Chen (ref. 13) and also of Roback and Johnson (ref. 14) indicate that the predictions show correct trends but are at best qualitative. It is the authors' opinion that further turbulence modeling for swirling flows should follow a more rigorous path rather than modifying "universal" turbulence constants. Two visible improvements of the standard k-ε model have been recently reported and are worth testing for rotating flows; these are the extended model of Chen and Kim (ref. 15) and the multiple-scale model of Chen (ref. 16). In the first model two time scales are introduced in the dissipation rate equation: (1) the production-range time scale $t_P = \rho k/P_K$; and (2) the dissipation-range time scale $t_D = k/\varepsilon$. With these scales the source term of the ε-equation is

$$S_\varepsilon = C_1 P_k \frac{\varepsilon}{k} - C_2 \rho \frac{\varepsilon^2}{k} + \frac{C_3 P_k^2}{\rho k} \tag{13}$$

or in terms of the time scales

$$S_\varepsilon = \frac{C_1 P_k}{t_D} - \frac{C_2 \rho \varepsilon}{t_D} + \frac{C_3 P_k}{t_P} \tag{14}$$

where

$$t_P = \frac{k\rho}{P_k}$$

$$t_D = \frac{k}{\varepsilon}$$

The last term represents the energy transfer rate from large-scale turbulence to small-scale turbulence and is controlled by the production-range time scale. The recommended constants are $C_1 = 1.15$, $C_2 = 1.9$, and $C_3 = 0.25$ (ref. 15). Results obtained with this model show significantly improved accuracy for swirling flows.

The second model, the multiple-scale k-ε model, has recently been successfully implemented by Chen (ref. 16). Following Kolmogorov (who postulated that the turbulence spectrum comprises independent production, inertial, and dissipation ranges), Hanjalic and Launder (ref. 17) have proposed a multiple-scale model in which separate transport equations are solved for the turbulence energy and dissipation rate across the spectrum. More recently Chen (ref. 13) has improved Launder's original formulation by ensuring an overall kinetic energy balance within the spectrum. The model includes two sets of k and ε equations for large-scale energetic eddies (P = production range) and for dissipative eddies (I = inertial or transfer range), as shown in figure 2. The source terms of the corresponding transport equations for this model are

$$\left.\begin{aligned} S_{kP} &= P_k - \rho\varepsilon_P \qquad (15) \\ S_{kI} &= \rho(\varepsilon_P - \varepsilon_I) \qquad (16) \end{aligned}\right\} \text{Production}$$

$$S_{\varepsilon P} = (C_{P_1} P_k - C_{P_2} \rho \varepsilon_P)/t_P \quad (17)$$

$$S_{\varepsilon I} = \rho(C_{I_1} \varepsilon_P - C_{I_2} \varepsilon_I)/t_P \quad (18)$$

Dissipation

where $t_P = k_P/\varepsilon_P$ is the production time constant and is defined differently than in Launder's model.

The coefficients are

$$\sigma_{kP} = \sigma_{kI} = 1 \quad (19)$$

$$\sigma_{\varepsilon P} = \sigma_{eI} = 1.22 \quad (20)$$

$$C_{P_1} = 1.6, \qquad C_{P_2} = 1.8 - 0.2 \frac{1 - k_I/k_P}{1 + k_I/k_P} \quad (21)$$

$$C_{I_1} = 1.15, \qquad C_{I_2} = 1.8 \frac{\varepsilon_I}{\varepsilon_P} \quad (22)$$

By using these model equations the Reynolds stresses are expressed according to

$$\rho\langle u_i', u_j' \rangle = -\mu_t \left[0.5 \left(\frac{\partial u_i}{\partial x_j} + \frac{\partial u_j}{\partial x_i}\right)\right] + \frac{2}{3} \rho k \delta_{ij} \quad (23)$$

where

$$k = k_I + k_P \quad (24)$$

and the eddy viscosity is given by

$$\mu_t = C_\mu \rho (k_P + k_I) \frac{k_P}{\varepsilon_P} \quad (25)$$

with $C_\mu = 0.09$.

Results obtained with this model show significantly improved accuracy over the standard k-ε model (eqs. (2) and (3)), have good prospects in rotating-flow applications, and represent a logical extension of this work.

FLUID INJECTION AND TURBULENCE MODEL RESULTS

Control of the integral, average circumferential velocity can lead to control of instabilities in rotating machines (Benkert and Wachter (ref. 18), Miller (ref. 19)); swirl brake and antiswirl applications (Kirk (ref. 20)); swirl and injection (Brown and Hart (ref. 21) and Bently and Muszynska (ref. 3));

injection (Hendricks (ref. 22)); friction and wall surface control (Nelson and Nguyen (ref. 4) and Von Pragenau (ref. 23)); preswirl (Childs (ref. 7)).

Fluid Injection

The fluid injection geometry is given in figure 3. Tam et al. (ref. 5) found that for a dynamic eccentricity of 0.8 with precessional speed equal to rotor speed, tangential fluid injection from four jets (at 0°, 90°, 180°, and 270°) angled at 3:1 (72°) significantly increases both direct, $K_D = K - M[\omega_p - (\lambda \mp \lambda_e)\omega_R]^2$, and quadrature, $K_Q = D[\omega_p - (\lambda \mp \lambda_e)\omega_R] - K_{xy}$, dynamic stiffnesses but that radial injection tends to be unstable (fig. 4). Tam also found that above 450 rad/s injection against the angle of rotation (-3:1, or -72°) produces larger quadrature dynamic stiffness but smaller direct stiffness than injection in the direction of rotation.

In the present study fluid injection against rotation at -1:1 (-45°) first produced an increase in dynamic stiffness (to 350 rad/s) and then decreased it to significantly less than that for injection with rotation at 1:1 (45°). However, for either case the dynamic stiffness was larger than Tam (ref. 5) found for injection at ±3:1 (±72°). This implies the existence of an optimum injection angle. The quadrature dynamic stiffness for injection against rotation at -1:1 (-45°) increased significantly with rotor speed, surpassing the other injection results. This implies enhanced configuration stability when fluids are injected against rotation. Figure 5 provides some qualitative details of the flowfield at L/4, L/2 - E, L/2, L/2 + E, and 3L/4, where L is the configuration length and E = L/20. The rotor speeds selected were 245 and 532 rad/s (2344 and 5085 rpm)[1] with fluid injection at an angle of 1:1 (45°) both against and in the direction of rotation (figs. 5(a) to (d), respectively). Preswirl was not considered. Note the zones of secondary flow, and in particular note the forward recirculation along the axis of rotation; the intensity of these zones increased when injection was against rotation and proportional to rotor speed. Note the emergence of discontinuous circumferential secondary flow zones at the higher rotor speed. It appears that with 1:1 injection the circumferential component was sufficiently weak to permit flow reattachment but the radial component was strong enough to "block the flow" and force fluid to recirculate upstream. Such secondary flows have not been found experimentally but have some parallel in the pocket bearing visualization work of Braun (private communication).

Comparing figures 4 and 5 indicates that at reduced rotor speeds injection against rotation enhanced the secondary flow zone, reducing the integral average circumferential velocity and increasing direct and quadrature dynamic stiffness. However, at the higher rotor speeds injection against rotation decreased direct but increased quadrature dynamic stiffness. This suggests that stiffness and damping could be decoupled in designing seals and bearings. Although injection angle and mass flow are important, other parameters such as clearance, radius, static eccentricity, rotor speed, and fluid properties remain to be investigated.

---

[1]The working fluid is bromotrifluoromethane ($CBrF_3$), the shaft diameter is 7.7 cm, and at these rotational speeds the Reynolds numbers simulate SSME class seals.

Turbulence Modeling

To investigate how turbulence modeling affects dynamic seal flows with inlet swirl, three models were used: Prandtl, standard k-ε, and modified k-ε. The steady three-dimensional Navier-Stokes equations using the PHOENICS solver (ref. 24) provided numerical results. The configuration and parameters are given in figure 6. The effective viscosity at three locations, 90° from the maximum clearance, approaching maximum clearance, and approaching minimum clearance is shown in figure 7. In most instances the general character of the profile was M-shaped. The peaks were prominant for the Prandtl model and underpredict the secondary flow zones as shown in figures 8 at L/8 and L/4 for a rotor speed of 5085 rpm, no preswirl, and no injection. The peaks were highest in the maximum clearance zone and nearly the same at 90° but lower when approaching the minimum clearance, indicating possible relaminarization[2] of the flowfield within the minimum clearance region as postulated by Braun et al. (ref. 25).

The standard k-ε model also peaked but at a reduced magnitude and tended to overpredict secondary flow zones. It was postulated that the modified k-ε model, incorporating the Richardson parameter ($Ri = (k/\varepsilon)^2 \left|(u_\theta/r^2)\right| dru_\theta/dr$ (eq. (12)) and producing results bounded by the other two models, would more accurately predict secondary flows and effective viscosity. In the absence of secondary flows turbulence production exceeded dissipation from the shaft to the wall (i.e., the Richardson parameter was negative and decreased, fig. 9(a); in some instances it may achieve a magnitude of 5). With secondary flows present, the Richardson parameter was first negative and decreasing but near the wall it abruptly increased and became positive (fig. 9(b)), indicating that turbulent dissipation exceeded production. This was also the region of secondary flow where direct and quadrature dynamic forces enhanced stability, implying that regions of positive Richardson parameter improved rotor stability.

Regions of positive and negative Richardson parameters, so called Richardson flux, are illustrated in figure 10, along with circumferential velocity at L/4 from inlet and L/4 from exit for rotor speeds of 3252 and 5085 rpm and preswirl with and against rotation; the modified k-ε model was used. The positive Richardson parameter zones are closely associated with regions of secondary flows, with negative zones being void of secondary flows. Note, however, that for both 3252 and 5085 rpm with preswirl against rotation, the Richardson flux became negative but the secondary flow zone persisted. The strength of these secondary flow zones depends among other things on eccentricity and could produce negative Richardson parameters at smaller eccentricities. However, as the shaft moves toward the housing, positive Richardson parameters

---

[2]Relaminarization within a flowfield approaching the minimum clearance, in particular near the rotor, would significantly reduce both the viscous forces and their perturbations within the minimum clearance, implying enhanced stability: The turbulent flowfield outside this zone, with viscous forces an order of magnitude or more larger, would be rebuffed or turned around, as in secondary flow that numerically has been shown to occur. A superlaminar flow could also be engendered in the same manner, and the flowfield would appear to be similar. Downstream of the minimum clearance the flow would then be characterized by transition from laminar to turbulent flows with flow separations or cavitations with either turbulent or superlaminar flows.

could be produced (i.e., first turbulent production exceeds damping, then turbulent damping exceeds production). The respective forces would tend to be first destabilizing and then stabilizing, causing drift followed by an abrupt movement of the shaft toward the centered position (i.e., an instability quench). This type of oscillation is apparently commonplace in turbomachinery and was pointed out to the authors by Childs (ref. 26).

It is interesting to note that the direct dynamic stiffness forces predicted by the standard $k-\varepsilon$ model were greater than those predicted by the modified $k-\varepsilon$ model for preswirl against rotation (fig. 11(a)). However, there was practically no difference in the quadrature dynamic forces (fig. 11(b)). At this time, we have no explanation for this result.

In comparing direct and quadrature dynamic forces, for the modified $k-\varepsilon$ model, the direct dynamic stiffness was less and had a larger negative slope for preswirl against rotation than for preswirl with rotation (fig. 12(a)). But the quadrature dynamic stiffness was greater and had a larger positive slope for preswirl against rotation than for preswirl with rotation (fig. 12(b)). With the formalization of the measurements of Morrison et al. (refs. 27 and 28), incorporation of the two-region model, and comparison to other Navier-Stokes solvers, the characterization of turbulence may be possible.

SUMMARY OF RESULTS

In this paper some effects of fluid injection into high-shear flows are discussed, and three turbulent models used to assess high-shear flows such as those in seals or bearings are examined.

Injection at 1:1 (45°) engendered a recirculating zone upstream of the injection plane and increased direct dynamic stiffness (magnitude and slope) over that for injection at 3:1 (72°). For injection at 1:1 the quadrature dynamic stiffness was negative at low speeds (unstable) and became positive at high speeds with a rather large slope for injection against rotation. These results suggest that designing for stiffness or damping may be configuration specific; further, variable injection angle and velocity could become the basis of a practical dynamic control system (i.e., the increase in stiffness is important to hydrostatic bearings).

Of the three models tested (Prandtl, standard $k-\varepsilon$, and modified $k-\varepsilon$) the Prandtl model tended to underpredict and the standard $k-\varepsilon$ tended to overpredict secondary flow zones; the modified $k-\varepsilon$ model was postulated to provide better results.

The standard $k-\varepsilon$ model tended to overpredict direct dynamic stiffness when compared with the modified $k-\varepsilon$ model; however, there was no change in quadrature dynamic stiffness.

The M-shaped effective viscosity profiles suggest significant production of turbulence near the rotor at about 25 percent of the clearance and a lesser peak near the stator at about 75 percent of the clearance. The effective viscosity and peaks were maximum near the maximum clearance and diminished in the convergence zone, suggesting the possibility of relaminarization or superlaminar flow. With viscous forces reduced in the minimum clearance region and

large in the turbulent flowfield outside this region, a physical model for secondary flows could be developed.

Without secondary flows the Richardson parameter was usually negative and decreased from the rotor to the stator; with secondary flows it first decreased and then increased, becoming positive near the stator and within the zone of secondary flow. A positive Richardson parameter implies that turbulent damping exceeds production, suggesting that designs where dissipation exceeds production near the stator are stable. As the rotor approaches the stator, an unstable rotor can engender secondary flow patterns that quench the instability; this usually implies that the Richardson parameter near the stator changes from negative to positive and provides an explanation of a common class of turbomachine oscillations cited by Childs.

REFERENCES

1. Muszynska, A; Franklin, W.D.; and Bently, D.E.: Rotor Active "Anti-Swirl" Control. 11th Biennial Conference on Mechanical Vibration and Noise. Sept. 27-30, 1987, Boston, MA. Vol. 2, "Rotating Machinery Dynamics."

2. Muszynska, A.; and Bently, D.E.: Anti-Swirl Arrangements Prevent Rotor/Seal Instability. Thermofluid Dynamics of Rotating Machinery, 2nd ASME/JSME Thermal Engineering Conference, Honolulu, HI, 1987, pp. 127-134.

3. Bently, D.E., Muszynska, A., and Hendricks, R.C., eds., 1986. "Instability in Rotating Machinery," Symposium Proceedings, NASA CP-2409.

4. Nelson, C.C. and Nguyen, D.T., 1986. "Comparison of Hirs' Equation with Moody's Equation for Determining Rotordynamic Coefficients of Annular Pressure Seals," ASME Paper 86-Trib-19, (see also Rotordynamic Instability Problems in High Performance Turbomachinery - 1986, NASA CP-2443, 1986, pp. 189-203).

5. Tam, L.T., Przekwas, A.J., Muszynska, A., Hendricks, R.C., Braun, M.J., and Mullen, R.L., 1987. "Numerical and Analytical Study of Fluid Dynamic Forces in Seals and Bearings," 11th Biennial Conference on Mechanical Vibration and Noise, Sept. 27-30, 1987, Boston, MA, Vol. 2, "Rotating Machinery Dynamics," pp. 359-370.

6. Nordman, R., Dietzen, F.J., and Weiser, H.P., 1987. "Calculation of Rotordynamic Coefficients and Leakage for Annular Gas Seals by Means of Finite Difference Techniques, 11th Biennial Conference on Mechanical Vibration and Noise, Sept. 27-30, 1987, Boston, MA, Vol. 2, "Rotating Machinery Dynamics," pp. 351-357. (See also Dietzen, F.J.; and Nordman, R., Calculating Rotordynamic Coefficients of Seals by Finite Difference Techniques. NASA CP-2443, 1986, pp. 77-98.)

7. Childs, D.W., 1983. "SSME HPFTP Interstage Seals: Analysis and Experiments for Leakage and Reaction-Force Coefficients," NASA CR-170876.

8. Launder, B.E. and Spalding, D.B., 1972. Mathematical Models of Turbulence, Pergamon Press.

9. Rodi, W., 1979. "Influence of Buoyancy and Rotation on Equations for the Turbulence Length Scale," 2nd Symp. on Turbulent Shear Flows.

10. Bradshaw, P., 1976. "The Effects of Streamwise Curvature on Turbulent Flow," AGARD-AG-169, AGARD, Paris, France.

11. Lakshminarayana, B., 1985. "Turbulence Modelling for Complex Shear Flows," AIAA Paper 85-1652.

12. Launder, B.E., Priddin, C.H., and Sharma, B.I., 1977. "The Calculation of Turbulent Boundary Layers on Spinning and Curved Surfaces," Journal of Fluids Engineering, Vol. 99, pp. 231-239.

13. Chen, C.P., 1986. "Calculation of Confined Swirling Jets," Communications in Applied Numerical Methods, Vol. 2, pp. 333-338.

14. Roback, R., and Johnson, B.V., 1983. "Mass Momentum Turbulent Transport Experiments With Confined Swirling Coaxial Jets," NASA CR-168252.

15. Chen, Y.S. and Kim, S.W., 1986. "Computation of Turbulent Boundary Layer Flows With an Algebraic Stress Turbulence Model," NASA CR-178967.

16. Chen, C.P., 1985. "Confined Swirling Jet Predictions Using a Multiple-Scale Turbulence Model," NASA CR-178484.

17. Hanjalic, K., Launder, B.E., and Schiestel, R., 1980. in Turbulent Shear Flows, p. 36.

18. Benkert, H. and Wachter, J., 1980. "Flow Induced Spring Coefficients for Laybrinth Seals for Applications in Rotordynamics," Rotordynamic Instability Problems in High-Performance Turbomachinery - 1980, NASA CP-2133, pp. 189-212.

19. Miller, E.H., 1983. "Rotor Stabilizing Labyrinth Seal for Steam Turbines," U.S. Patent 4,420,161.

20. Kirk, R.G., 1987. "Influence of Disk Leakage Path on Labyrinth Seal Inlet Swirl Ratio," Rotordynamic Instability Problems in High-Performance Turbomachinery - 1986, NASA CP-2443, pp. 225-236.

21. Brown, R.D. and Hart, A., 1986. "A Novel Form of Damper for Turbomachinery," Rotordynamic Instability Problems in High-Performance Turbomachinery - 1986, NASA CP-2443, pp. 325-347.

22. Hendricks, R.C., 1987. "Straight Cylindrical Seal for High Performance Turbomachines," NASA TP-1850.

23. Von Pragenau, G.L., 1982. "Damping Seals for Turbomachinery," NASA TP-1987.

24. Spalding, D.B., 1981. "General Computer Program for Multi-Dimensional One- and Two-Phase Flow," Mathematics and Computers in Simulations, Vol. 23, No. 3, pp. 267-276.

25. Braun, M.J., Batur, C., Rose, B., Ida, N., Hendricks, R.C., and Mullen, R.L., "A Non-Invasive Laser-Based Method in Flow Visualization and Evaluation in Bearings," Paper C188/87, I Mech E., pp. 37-46.

26. Childs, D.W.: Written discussion comments to be appended to ref. 4.

27. Morrison, G.L., Johnson, M.C., and Tatterson, G.B., 1988. "3-D Laser Anemometer Measurements in an Annular Seal," for presentation at International Gas Turbine and Aeroengine Congress & Exposition, June 5-9, 1988, Amsterdam, The Netherlands.

28. Morrison, G.L., Johnson, M.C., and Tatterson, G.B., 1988. "3-D Laser Anemometer Measurements in Labyrinth Seal," for presentation at International Gas Turbine and Aeroengine Congress & Exposition, June 5-9, 1988, Amsterdam, The Netherlands.

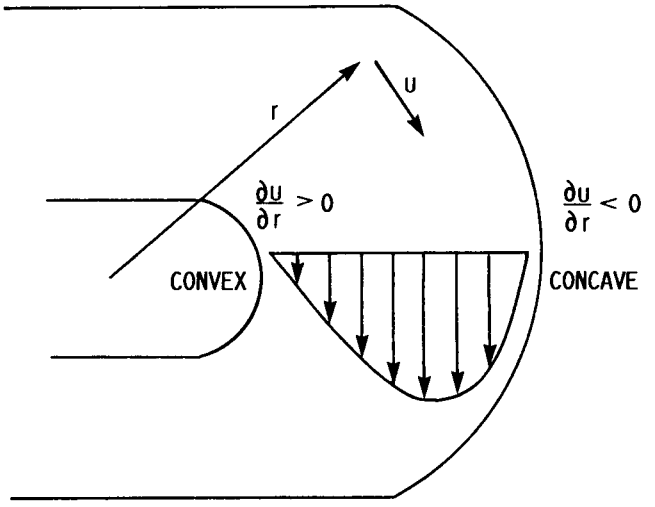

(A) CURVED CHANNEL FLOW.

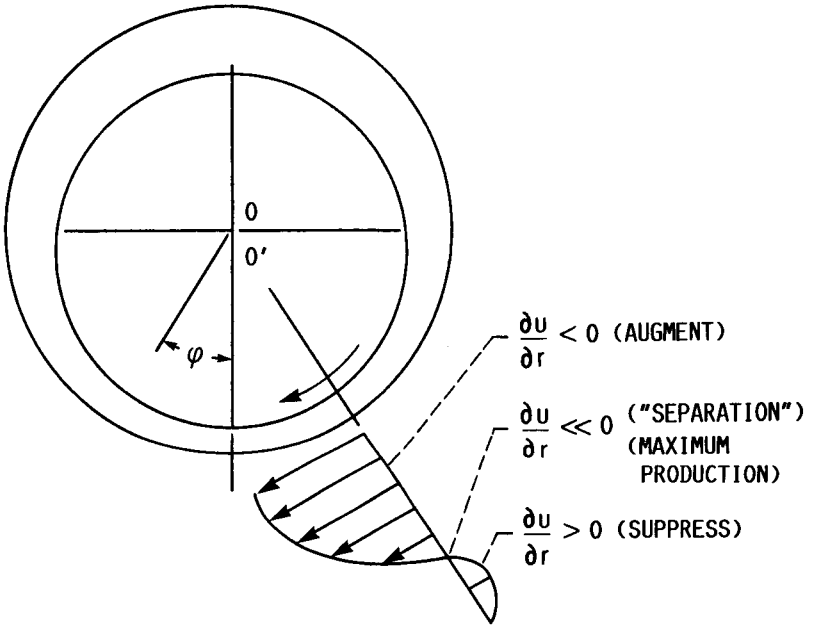

(B) PASSAGE WITH ROTATING SHAFT.

FIGURE 1. - SKETCHES OF TURBULENCE REDISTRIBUTION.

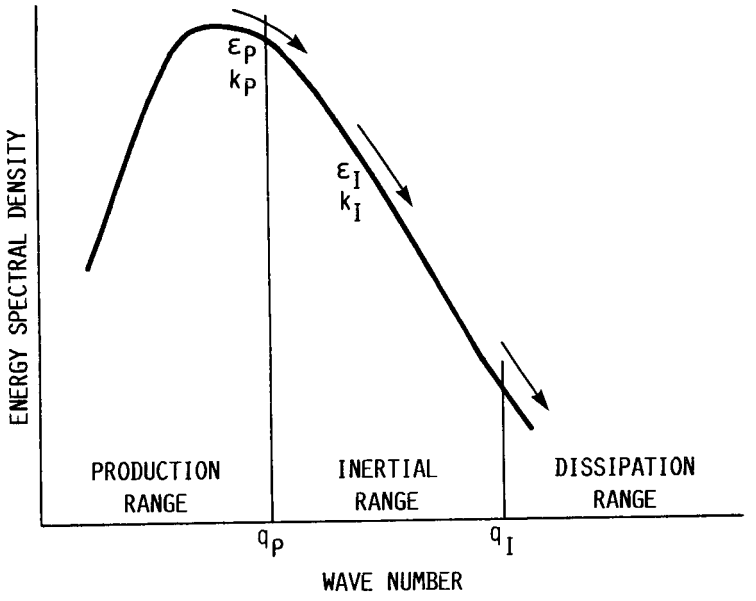

FIGURE 2. - PARTITIONED ENERGY SPECTRUM TURBULENCE MODEL.

INJECTION DIRECTION	INJECTION ANGLE, γ
WITH ROTATION	ARCTAN (3) AND (1)
RADIAL	0
AGAINST ROTATION	ARCTAN (-3) AND (-1)

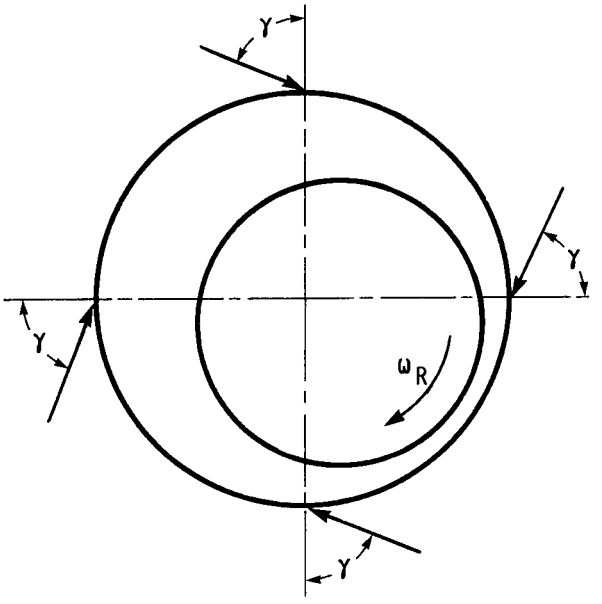

FIGURE 3. - INJECTION GEOMETRY AND OPERATING PARAMETERS. z = L/2.

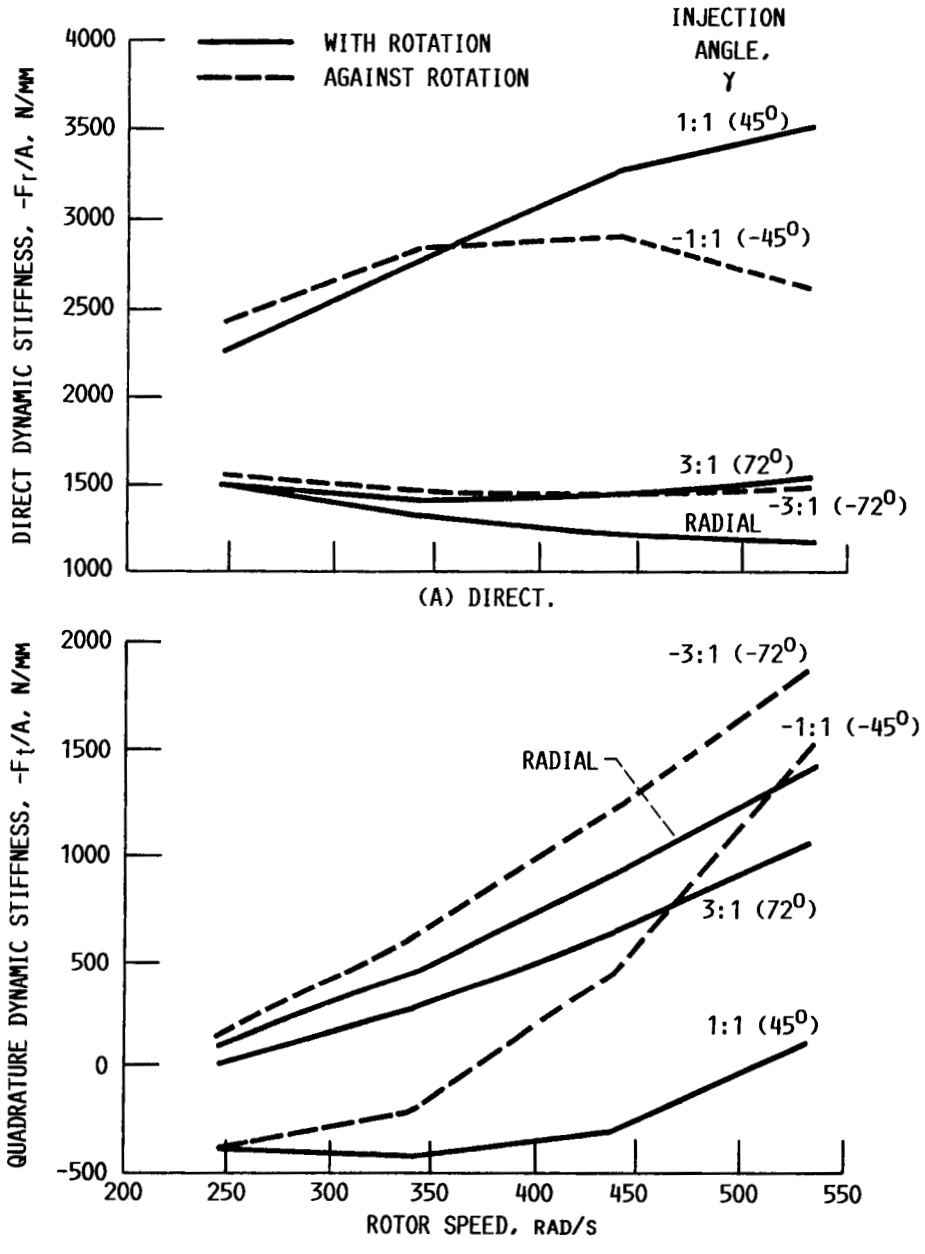

FIGURE 4. - DYNAMIC STIFFNESS FORCES FOR ±1:1 AND ±3:1 INJECTION ANGLES WITH AND AGAINST ROTATION AS A FUNCTION OF ROTOR SPEED, SYNCHRONOUS PERTURBATION, AND PRANDTL TURBULENCE MODEL, WITH DYNAMIC ECCENTRICITY/CLEARANCE RATIO A/c OF 0.8. (WORKING FLUID, HALON ($CBrF_3$); PRANDTL MIXING LENGTH TURBULENCE MODEL ONLY.)

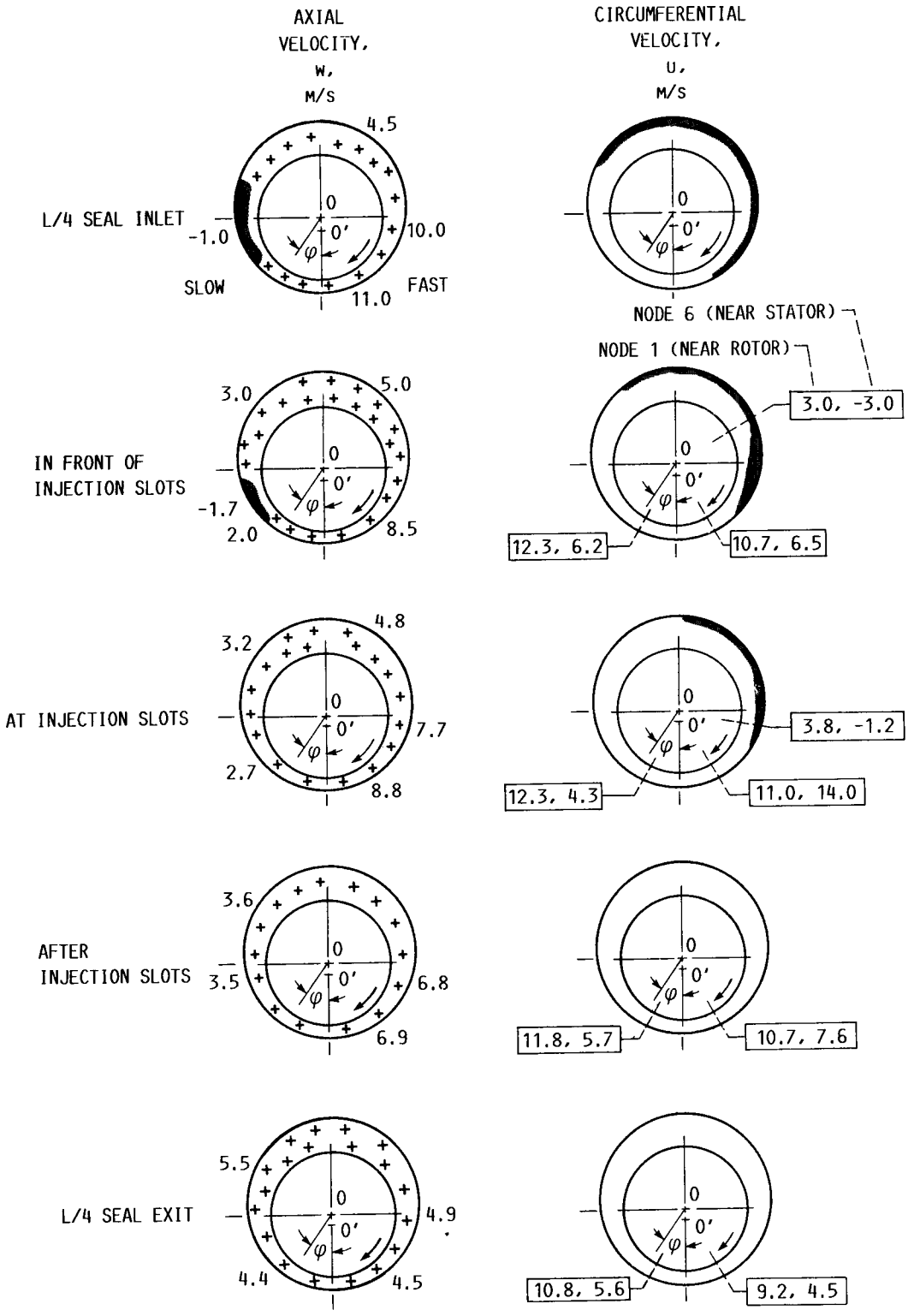

(A) ROTOR SPEED, 2344 RPM; INJECTION WITH ROTATION (1:1).

FIGURE 5. - QUALITATIVE AXIAL AND CIRCUMFERENTIAL FLOW VELOCITIES AT FIVE AXIAL CROSS SECTIONS (L/4, L/2 - E, L/2, L/2 + E, 3L/4) WITH A/c = 0.8. (PRANDTL MIXING LENGTH TURBULENCE MODEL.) + INDICATES $w > 0$.

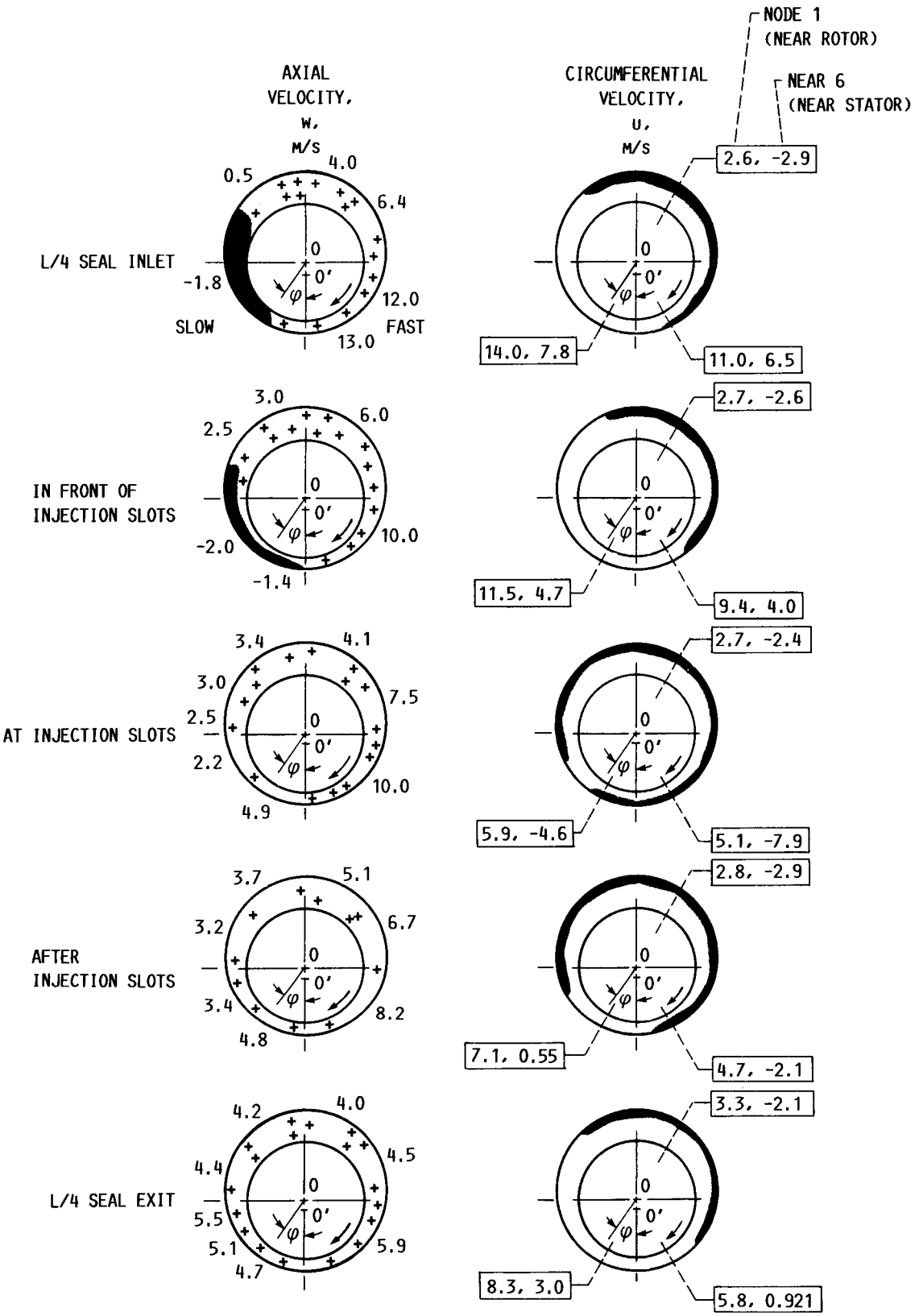

(B) ROTOR SPEED, 2344 RPM; INJECTION AGAINST ROTATION (-1:1).

FIGURE 5. - CONTINUED.

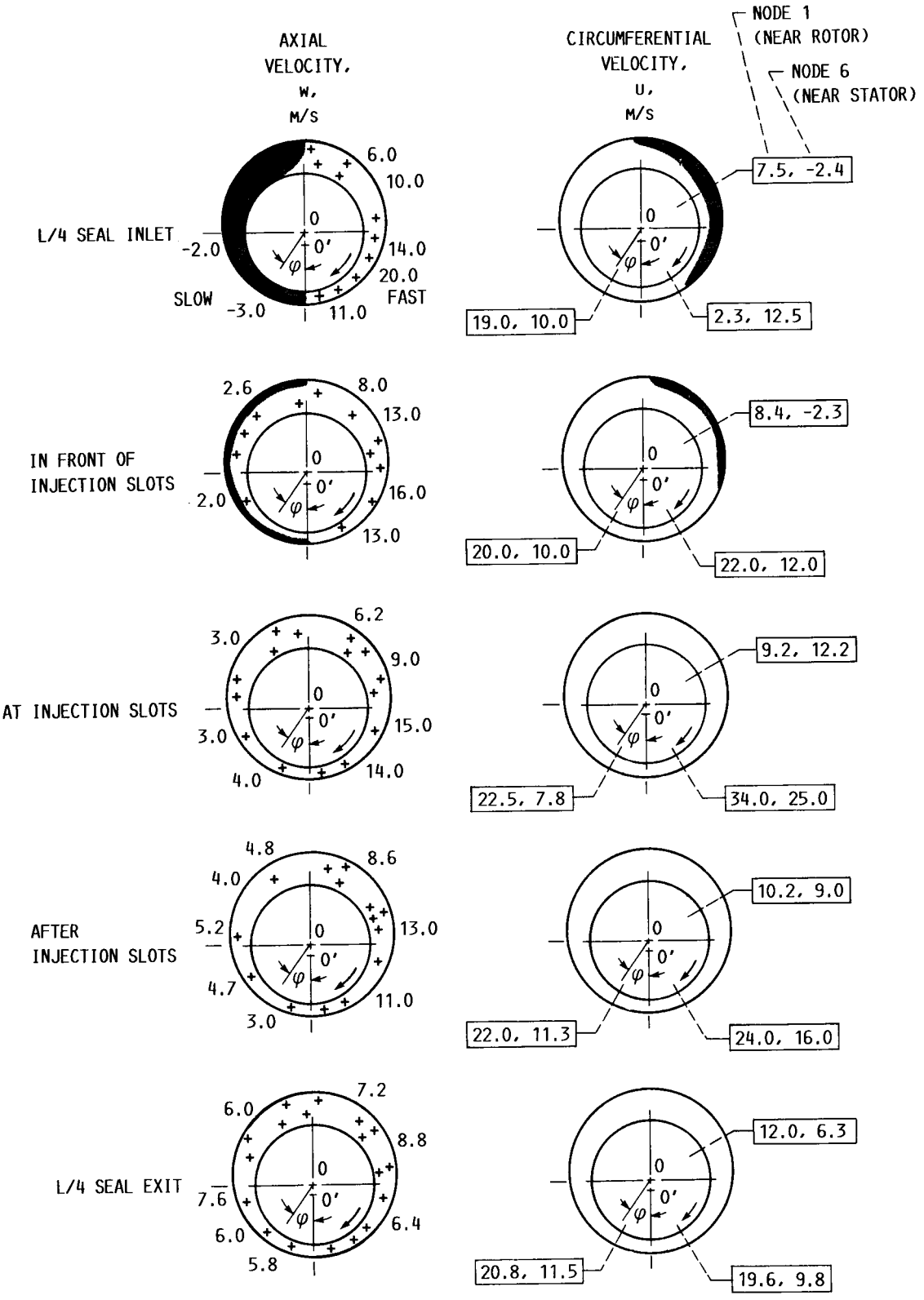

(C) ROTOR SPEED, 5085 RPM; INJECTION WITH ROTATION (1:1).

FIGURE 5. - CONTINUED.

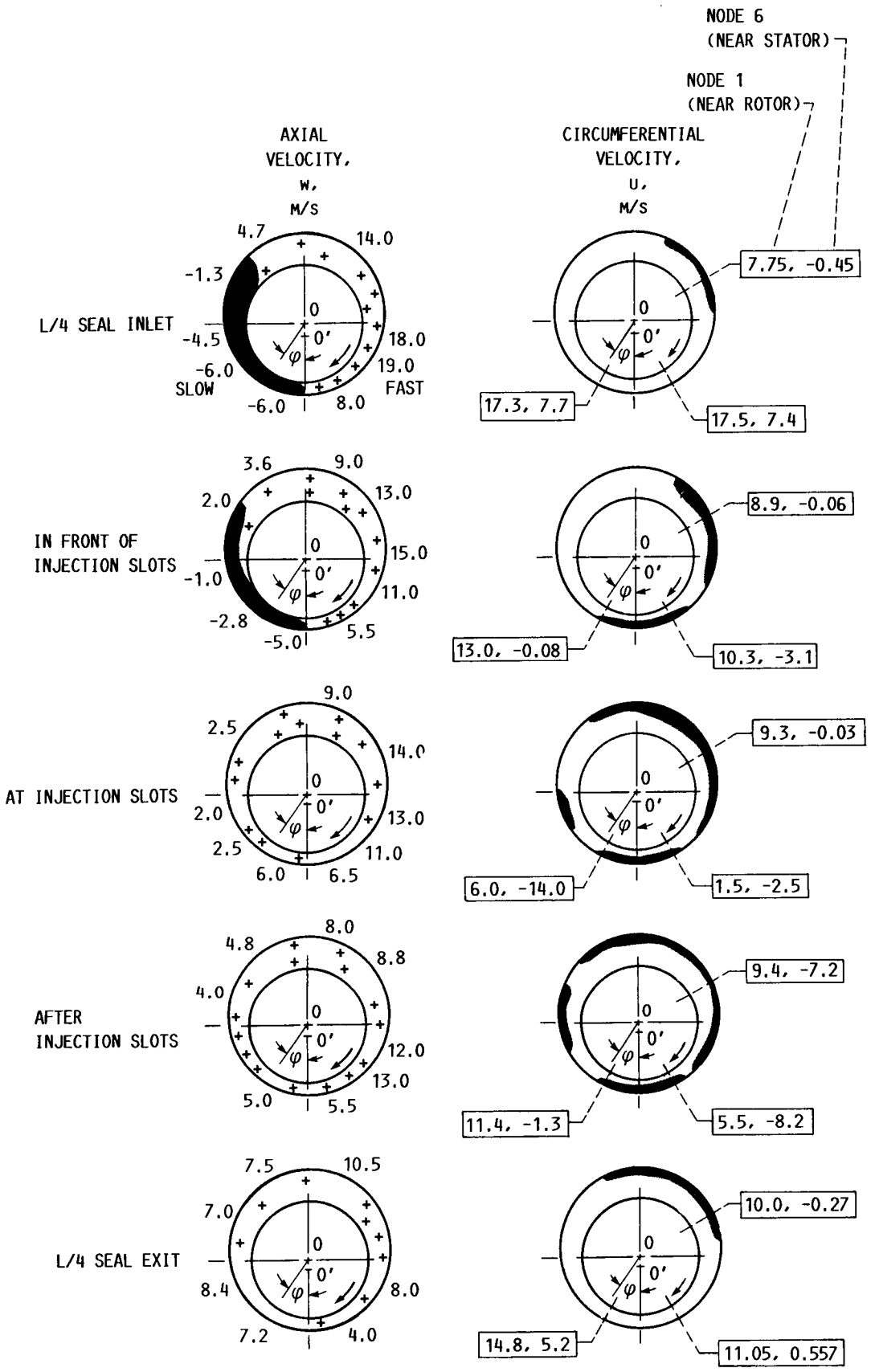

(D) ROTOR SPEED, 5085 RPM; INJECTION AGAINST ROTATION (-1:1).

FIGURE 5. - CONCLUDED.

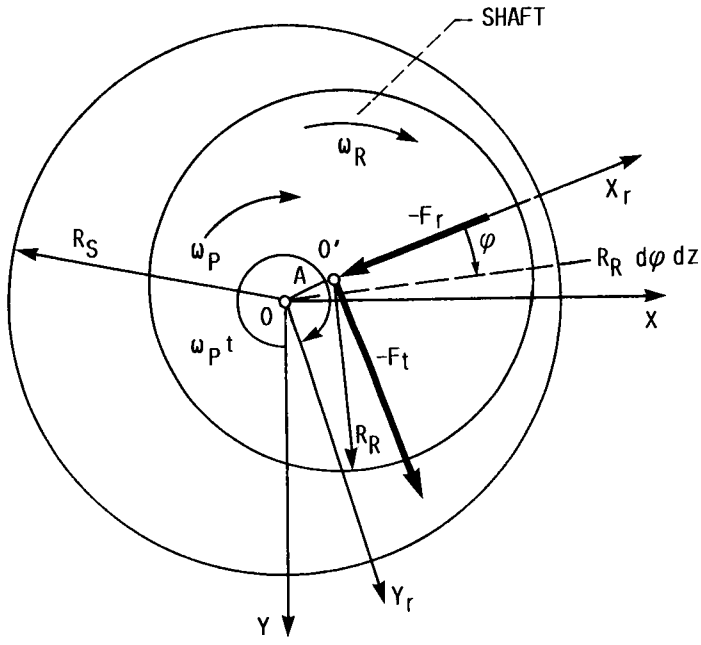

FIGURE 6. - SEAL CONFIGURATION AND PARAMETERS FOR SWIRL FLOWS.

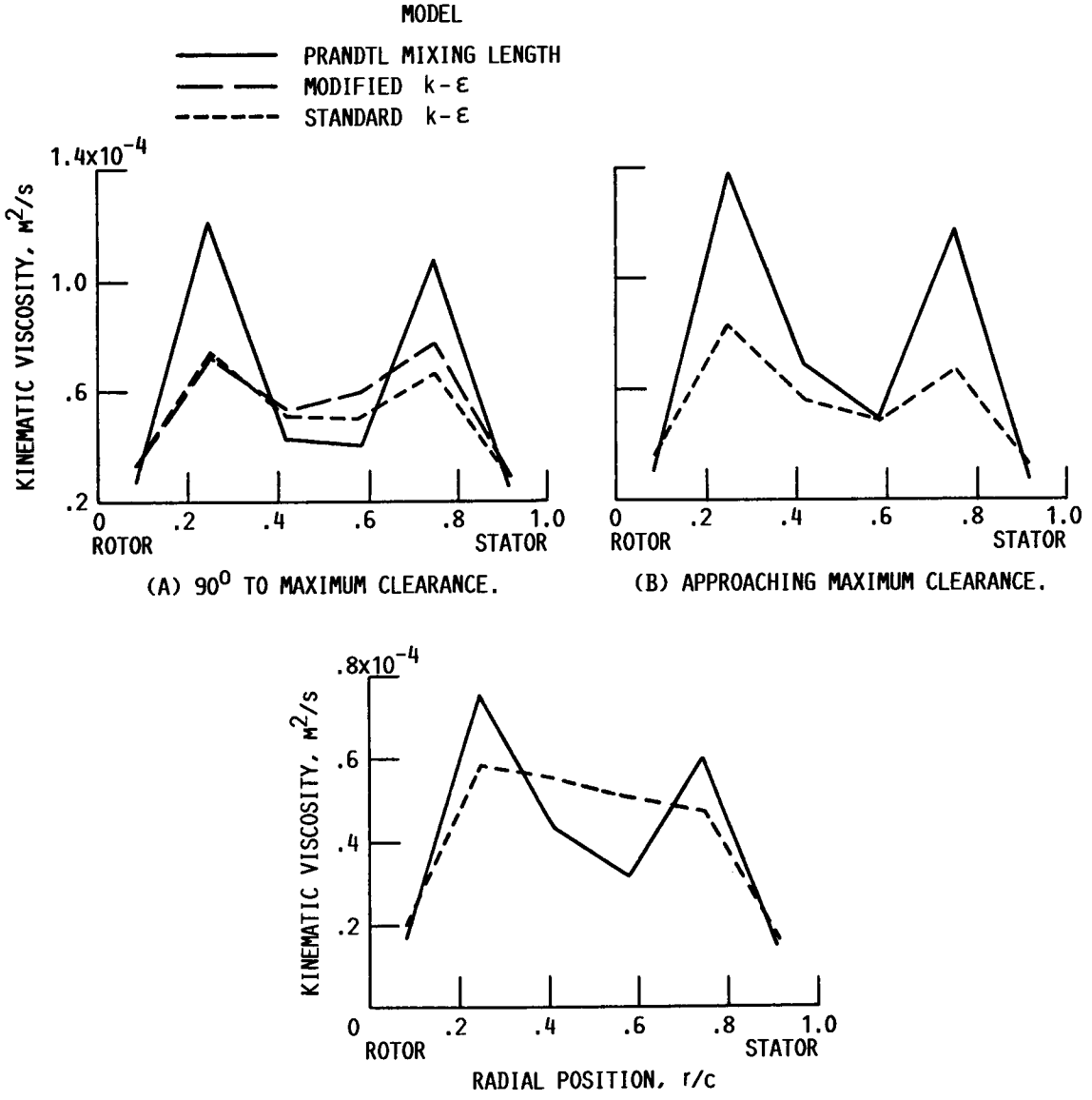

FIGURE 7. - EFFECTIVE VISCOSITY AS A FUNCTION OF RADIAL POSITION AT THREE CIRCUMFERENTIAL POSITIONS.

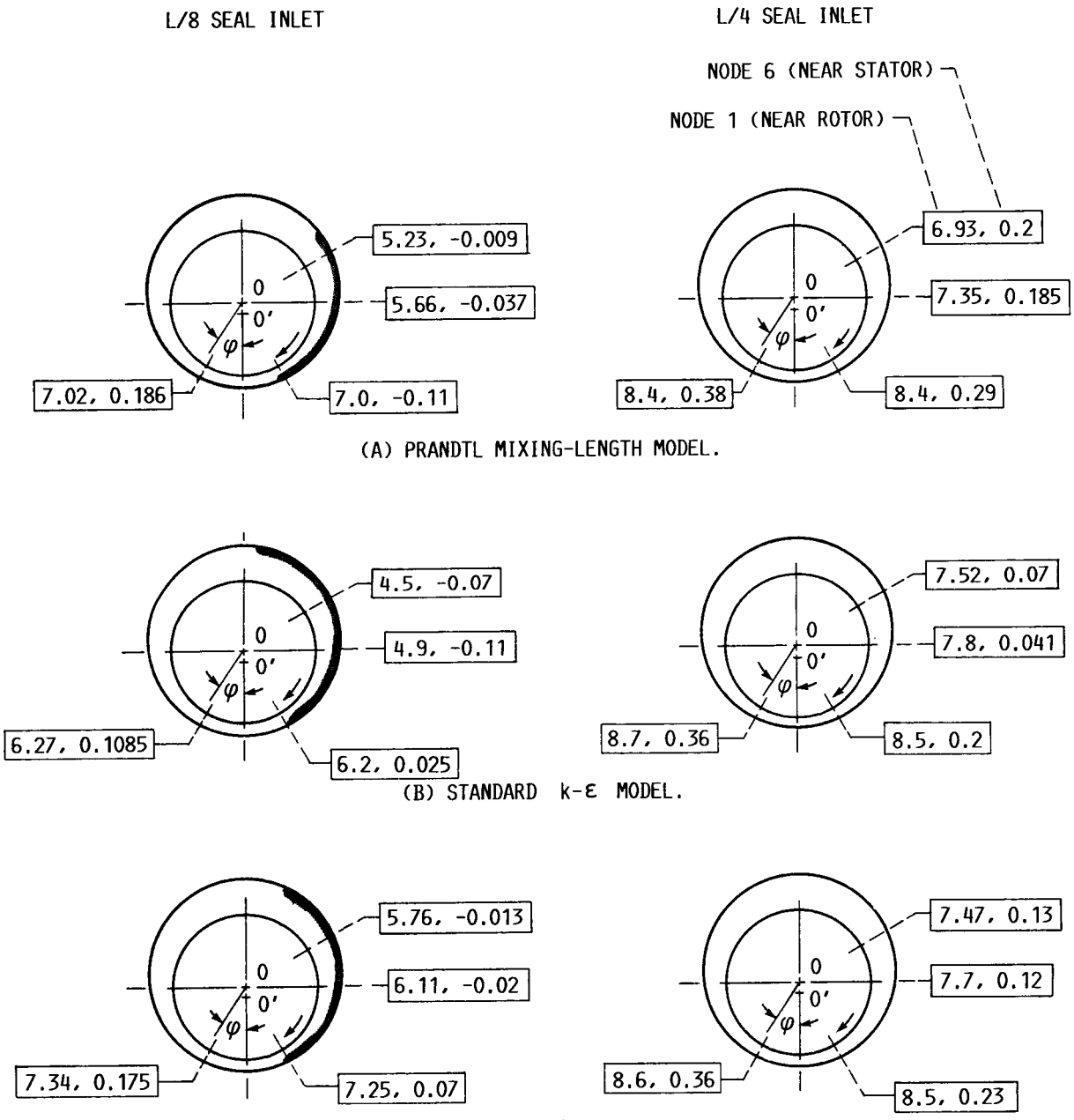

FIGURE 8. - ZONES OF SECONDARY FLOWS AND CIRCUMFERENTIAL VELOCITIES NEAR ROTOR AND STATOR FOR THREE TURBULENCE MODELS. ROTOR SPEED, 5085 RPM, NO PRESWIRL, AND NO INJECTION.

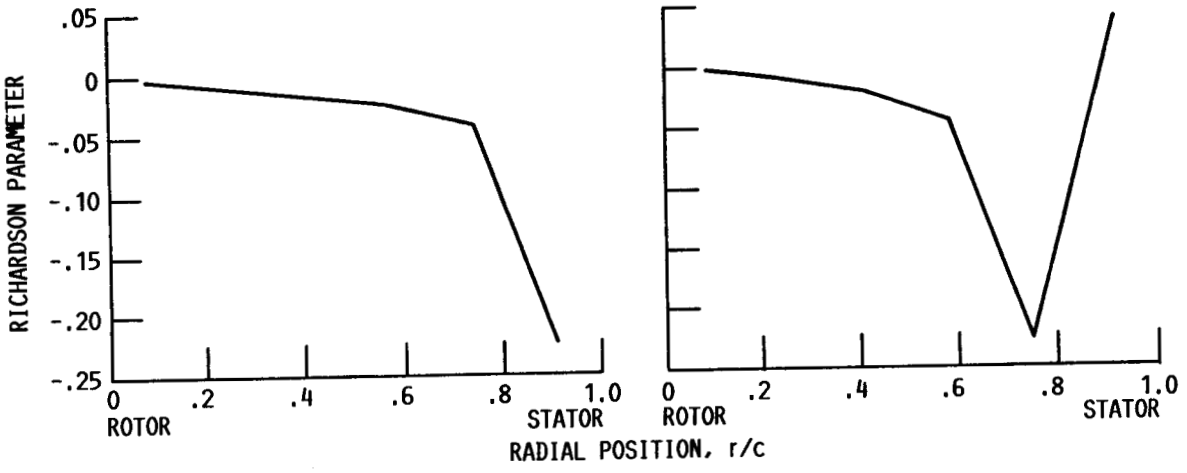

(A) NO SECONDARY FLOW. (B) SECONDARY FLOW ZONE NEAR STATOR.

FIGURE 9. - RICHARDSON PARAMETER AS A FUNCTION OF RADIAL POSITION. (LAUNDER MODEL.)

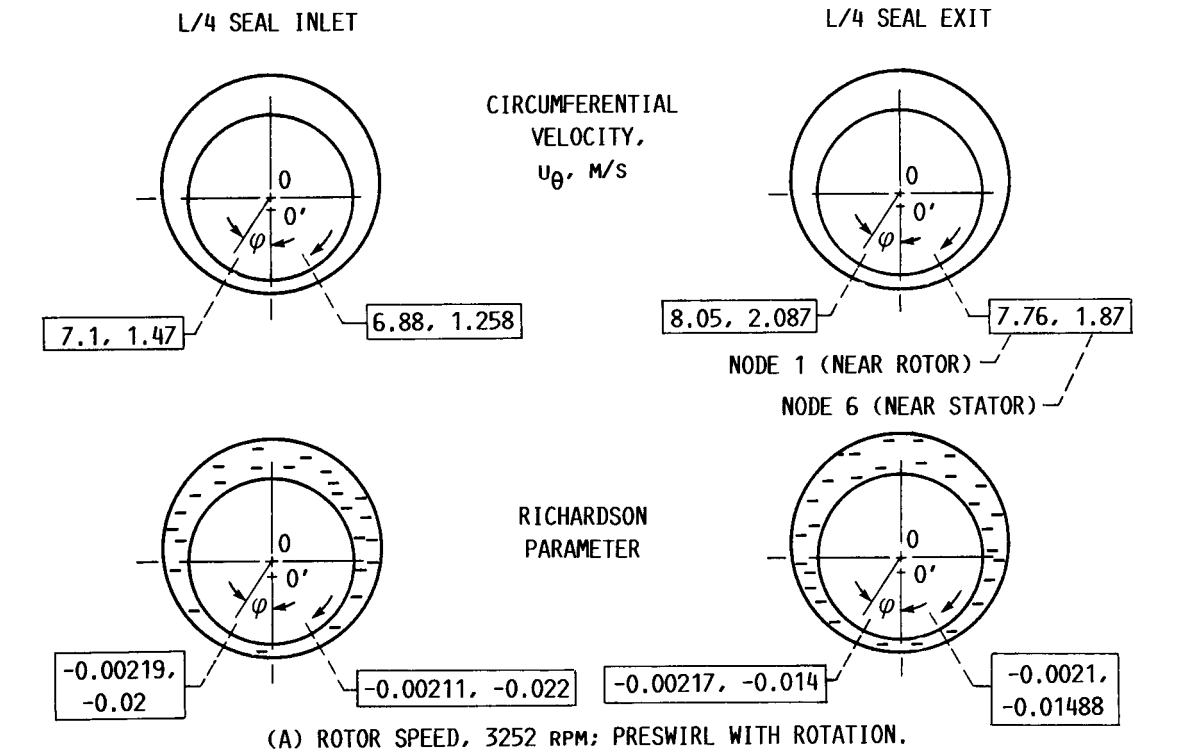

(A) ROTOR SPEED, 3252 RPM; PRESWIRL WITH ROTATION.

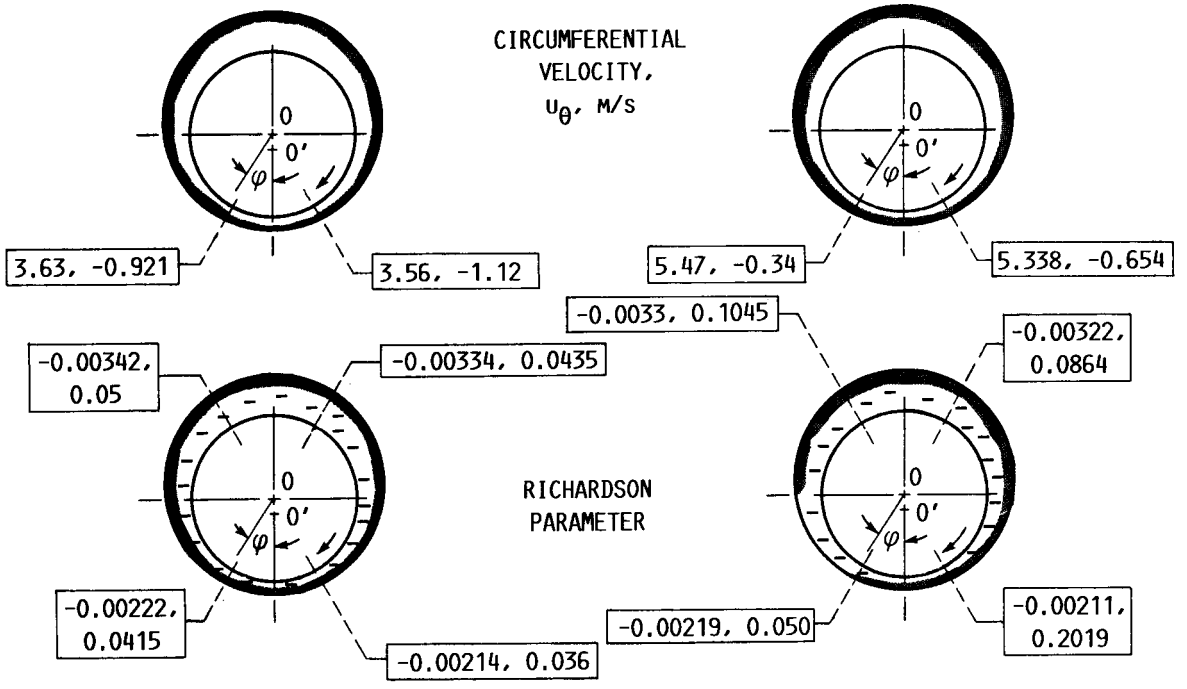

(B) ROTOR SPEED, 3252 RPM; PRESWIRL AGAINST ROTATION.

FIGURE 10. - QUALITATIVE CIRCUMFERENTIAL VELOCITIES AND VARIATIONS OF RICHARDSON PARAMETER WITHIN SEAL CROSS SECTION FOR SYNCHRONOUS PERTURBATION, A/c = 0.24, AND MODIFIED k-ε MODEL.

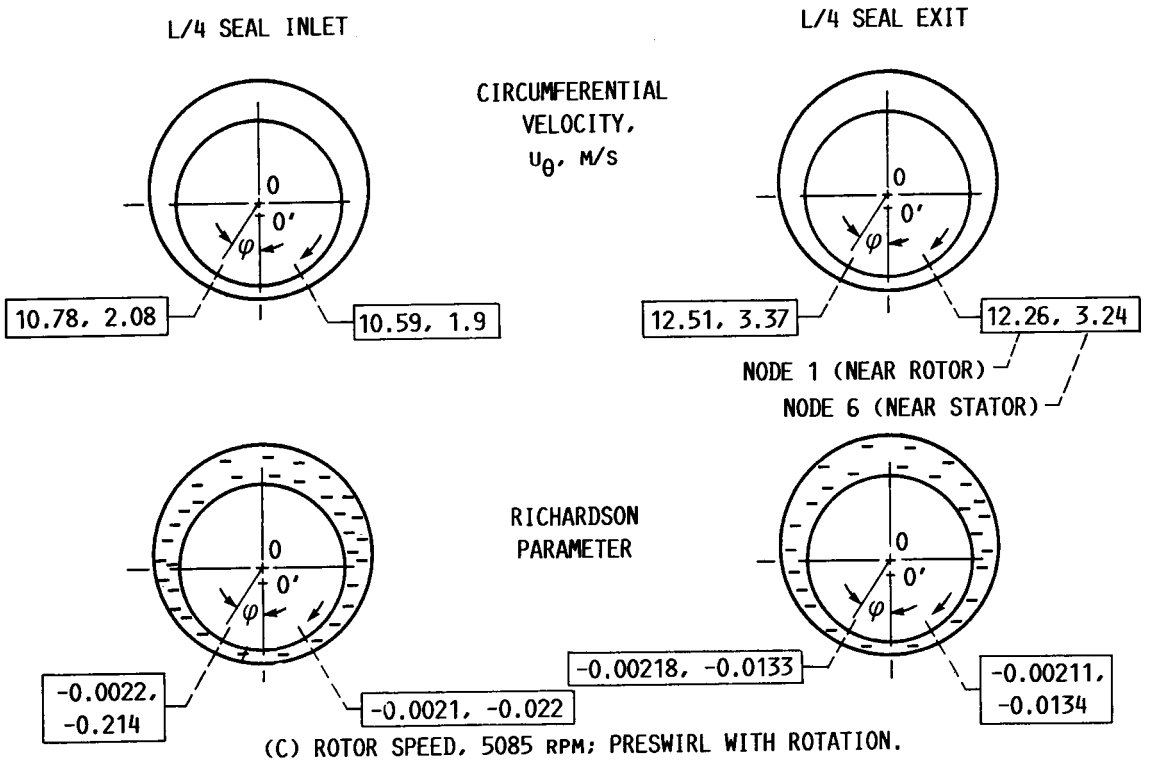

(C) ROTOR SPEED, 5085 RPM; PRESWIRL WITH ROTATION.

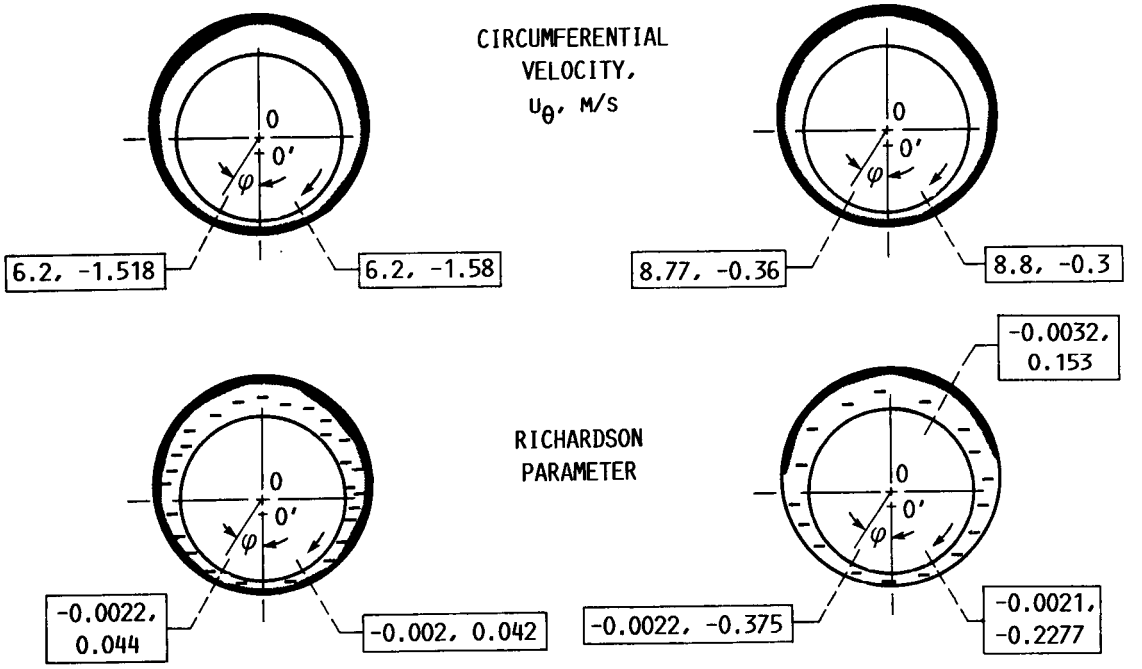

(D) ROTOR SPEED, 5085 RPM; PRESWIRL AGAINST ROTATION.

FIGURE 10. - CONCLUDED.

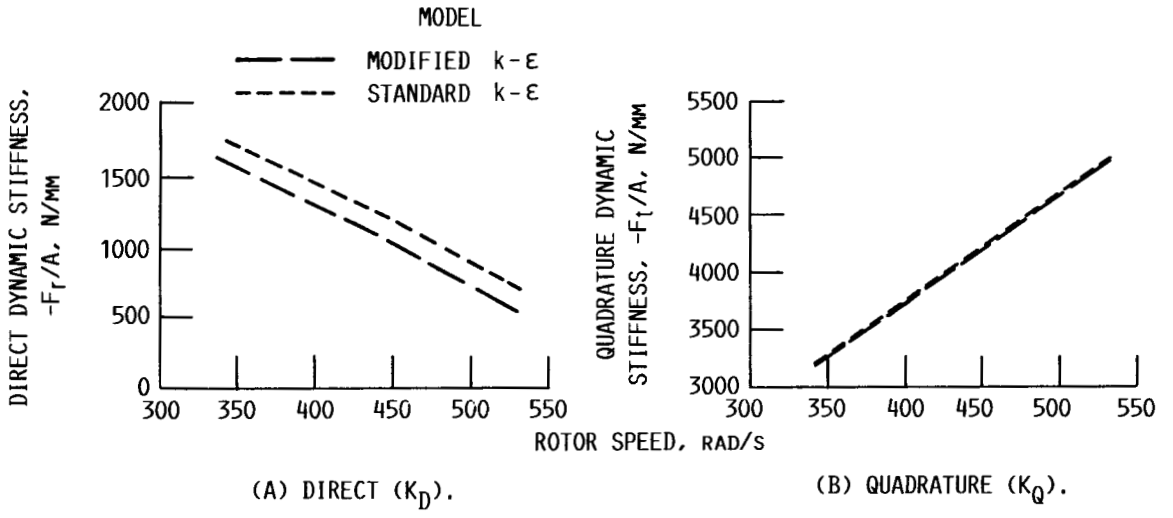

(A) DIRECT (K_D). (B) QUADRATURE (K_Q).

FIGURE 11. - DYNAMIC STIFFNESS FORCES USING STANDARD AND MODIFIED k-ε TURBULENCE MODELS AS A FUNCTION OF ROTOR SPEED, SYNCHRONOUS PERTURBATION, AND PRESWIRL AGAINST ROTATION. ξ = --. ($V_{PRESWIRL}/R_R\omega_R = \pm(1 - r/R_S)^{1/3}$.)

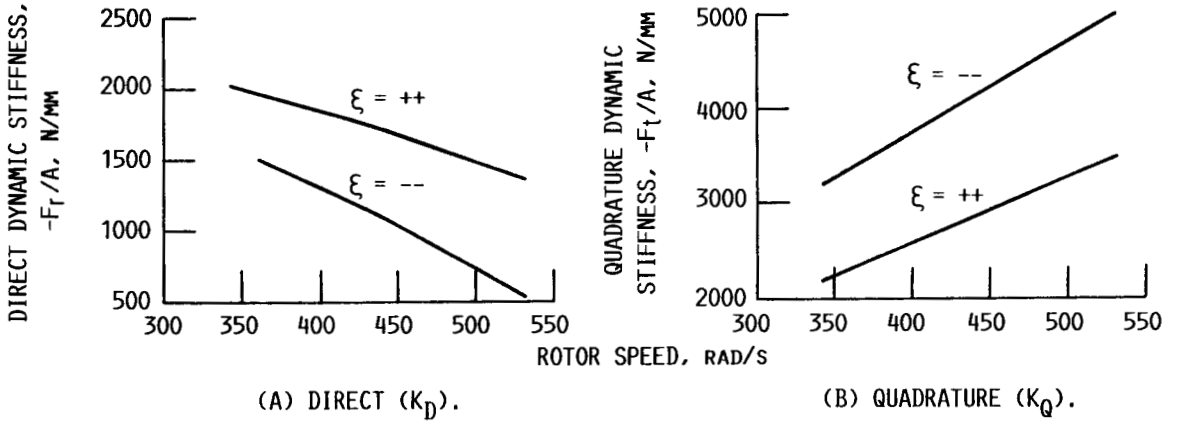

(A) DIRECT (K_D). (B) QUADRATURE (K_Q).

FIGURE 12. - DYNAMIC STIFFNESS FORCES USING MODIFIED k-ε TURBULENCE MODEL AS A FUNCTION OF ROTOR SPEED, SYNCHRONOUS PERTURBATION, AND PRESWIRL AGAINST AND WITH ROTATION. ($V_{PRESWIRL}/R_R\omega_R = \pm(1 - r/R_S)^{1/3}$.)

NASA
National Aeronautics and Space Administration

Report Documentation Page

1. Report No.	2. Government Accession No.	3. Recipient's Catalog No.
NASA TM-100779		

4. Title and Subtitle
Numerical Modeling of Multidimensional Flow in Seals and Bearings Used in Rotating Machinery

5. Report Date

6. Performing Organization Code

7. Author(s)
R.C. Hendricks, L.T. Tam, A. Przekwas, A. Muszynska, M.J. Braun, and R.L. Mullen

8. Performing Organization Report No.
E-3909

10. Work Unit No.
505-62-21

9. Performing Organization Name and Address
National Aeronautics and Space Administration
Lewis Research Center
Cleveland, Ohio 44135

11. Contract or Grant No.

13. Type of Report and Period Covered
Technical Memorandum

12. Sponsoring Agency Name and Address
National Aeronautics and Space Administration
Washington, D.C. 20546

14. Sponsoring Agency Code

15. Supplementary Notes
Prepared for the 2nd International Symposium on Transport Phenomena, Dynamics, and Design of Rotating Machinery, cosponsored by the ASME and JSME, Honolulu, Hawaii, April 4-6, 1988. R.C. Hendricks, NASA Lewis Research Center; L.T. Tam and A. Przekwas, CHAM, Huntsville, Alabama 35816; A. Muszynska, Bently Rotordynamics Research Corporation, Minden, Nevada 89423; M.J. Braun, University of Akron, Akron, Ohio 44325; R.L. Mullen, Case Western Reserve University, Cleveland, Ohio 44106.

16. Abstract
The rotordynamic behavior of turbomachinery is critically dependent on fluid dynamic rotor forces developed by various types of seals and bearings. The occurrence of self-excited vibrations often depends on the rotor speed and load. Misalignment and rotor wobbling motion associated with differential clearance have often been attributed to stability problems. In general, the rotative character of the flowfield is a complex three-dimensional system with secondary flow patterns that significantly alter the average fluid circumferential velocity. A multidimensional, nonorthogonal, body-fitted-grid fluid flow model is represented that describes the fluid dynamic forces and the secondary flow pattern development in seals and bearings. Several numerical experiments were carried out to demonstrate the characteristics of this complex flowfield. Analyses were performed by solving a conservation form of the three-dimensional Navier-Stokes equations transformed to those for a rotating observer and using the general-purpose computer code PHOENICS with the assumptions that the rotor orbit is circular (nonzero dynamic eccentricity) and that static eccentricity is zero. These assumptions have enabled a precise steady-state analysis to be used. Fluid injection from ports near the seal or bearing center increased fluid-film direct dynamic stiffness $K_D = K - M\omega^2(1 - \bar{\lambda} \pm \lambda_e)$ and, in some cases, significantly increased quadrature dynamic stiffness $K_Q = D\omega(1 - \bar{\lambda} \pm \lambda_e) - K_{xy}$). Under certain conditions K_Q was less than zero, implying instability (necessary but not sufficient condition) and geometric configuration dependency. Injection angle and velocity could be used for active rotordynamic control. Three turbulence models were tested: Prandtl mixing, standard $k-\varepsilon$, and modified $k-\varepsilon$. The Prandtl model overpredicted the secondary flow zone.

17. Key Words (Suggested by Author(s))	18. Distribution Statement
Seals Bearings Dynamics Flow	Unclassified - unlimited Subject Category 34

19. Security Classif. (of this report)	20. Security Classif. (of this page)	21. No of pages	22. Price*
Unclassified	Unclassified	30	A03

*For sale by the National Technical Information Service, Springfield, Virginia 22161